JCTC Journal of Chemical Theory and Computation

Article

pubs.acs.org/JCTC

Development of a "First Principles" Water Potential with Flexible Monomers: Dimer Potential Energy Surface, VRT Spectrum, and Second Virial Coefficient

Volodymyr Babin,*[,†] Claude Leforestier,*[,‡] and Francesco Paesani*[,†]

[†]Department of Chemistry and Biochemistry, University of California, San Diego, La Jolla, California 92093, United States

[‡]ICG-CTMM CC 15.01, Universite Montpellier II , 34095 Montpellier, Cedex 05, France

Supporting Information

ABSTRACT: The development of a "first principles" water potential with flexible monomers (MB-pol) for molecular simulations of water systems from gas to condensed phases is described. MB-pol is built upon the many-body expansion of the intermolecular interactions, and the specific focus of this study is on the two-body term (V_{2B}) representing the full-dimensional intermolecular part of the water dimer potential energy surface. V_{2B} is constructed by fitting 40,000 dimer energies calculated at the CCSD(T)/CBS level of theory and imposing the correct asymptotic behavior at long-range as predicted from "first principles". The comparison of the calculated vibration−rotation tunneling (VRT) spectrum and second virial coefficient with the corresponding experimental results demonstrates the accuracy of the MB-pol dimer potential energy surface.

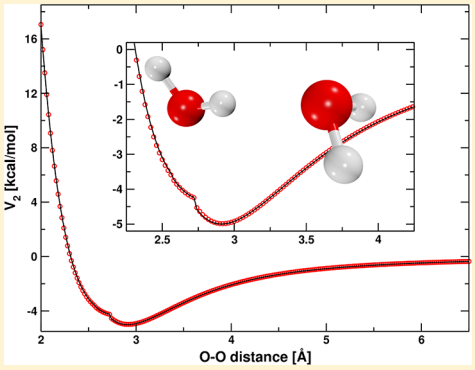

1. INTRODUCTION

The accurate description of intermolecular forces in increasingly larger systems remains an outstanding challenge in theoretical and computational chemistry.[1] This problem is well exemplified by the myriad of water models that have been developed over the last decades, including coarse-grained representations with no atomistic details (e.g., ref 2), classical parametrizations in terms of point charges and rigid bonds (see ref 3 for a recent review), and more sophisticated models that account for molecular flexibility (e.g., ref 4), electronic polarization (e.g., ref 5), and charge transfer (e.g., ref 6), none of which are, however, capable of consistently reproducing properties of water from the gas to the condensed phases. As a result, despite much recent progress, the molecular-level understanding of the behavior of water under different conditions and in different environments is still incomplete.[7−13] In general terms, the difficulties encountered in representing the interactions between water molecules arise from the subtle interplay of energetic and entropic contributions that shape the free-energy landscape associated with different rearrangements of the hydrogen-bond (HB) network. This implies that (1) correlated quantum chemistry methods such as the many-body perturbation theory and coupled cluster (currently considered as the gold standard for electronic structure calculations) are required for an accurate determination of the multidimensional Born−Oppenheimer (BO) potential energy surface (PES) and (2) nuclear quantum effects must be explicitly taken into account in molecular simulations carried out with ab initio representations of the underlying interactions in order to properly describe the fluctuations of the HB network from "first principles" without resorting to empirical and/or ad hoc approximations. Unfortunately, the high computational cost associated with correlated electronic structure methods effectively limits these types of calculations to relatively small water clusters (up to approximately six molecules). This limitation has motivated the development of more efficient approaches aiming at approximating the true BO PES over a range of energies sufficiently wide for realistic simulations of water across different phases.

As mentioned above, several atomistically resolved water models have been proposed in the literature.[14] With very few exceptions (most notably CC-pol,[15] WHBB,[16] and HBB2-pol[17]), the majority of these models contains a certain degree of empiricism that is used to reproduce a limited number of experimentally measured properties. Building on the many-body expansion of the interactions,[18] we have recently undertaken the development of a full-dimensional water potential (called MB-pol) entirely from "first principles" with the goal of accurately describing the properties of water following a bottom-up approach from the gas-phase dimer to condensed phase systems. The focus of this article (the first of a series describing the MB-pol potential), is on the two-body (2B) term, $V_{2B}(x_a,x_b)$, representing the interaction energy between two water molecules (a and b). $V_{2B}(x_a,x_b)$ is defined as the difference between the total energy of the dimer, $E(x_a,x_b)$, and the one-body (1B) energies of the two isolated molecules, $V_{1B}(x_a)$ and $V_{1B}(x_a)$

Received: October 1, 2013
Published: November 14, 2013

$$V_{2B}(x_a, x_b) = E(x_a, x_b) - V_{1B}(x_a) - V_{1B}(x_b) \quad (1)$$

Here, x_i collectively denotes the positions of all atoms belonging to the i-th water molecule. Following previous studies,[19,20] the $V_{1B}(x_i)$ of the MB-pol potential is represented by the spectroscopically accurate PES developed by Partridge and Schwenke.[21]

The article is organized as follows. The development of the MB-pol potential is described in Section 2. The accuracy of $V_{2B}(x_a,x_b)$ is assessed in Section 3 through the comparison of the calculated dimer vibration−rotation tunneling spectrum and second virial coefficient with the corresponding experimental data. Lastly, a summary highlighting the main findings and discussing future directions is given in Section 4.

2. MODEL DEVELOPMENT

2.1. "First Principles" Energies. The one-center asymptotic expansion,[22] as presented in eq 1 of ref 23, was used to compute the interaction energy between two water molecules at large separations. The coefficients for both induction and dispersion contributions were taken from ref 24. The short-range reference energies were computed at the coupled cluster level including single, double, and iterative triple excitations, CCSD(T). The MOLPRO program[25] was used for all calculations, and the counterpoise method[26] was applied to remove the basis set superposition error (BSSE).

The calculations were carried out with the augmented correlation-consistent polarized-valence triple (aug-cc-pVTZ) and quadruple-ζ (aug-cc-pVQZ) basis sets[27] supplemented by an additional set of 3s3p2d1f midbond functions[28] with exponents equal to (0.9, 0.3, 0.1) for sp, (0.6, 0.2) for d, and 0.3 for f, placed at the center of mass (COM) of each dimer configuration. The interaction energies were extrapolated to the complete basis set (CBS) limit using the following two-point formula[29,30]

$$V_2^X = V_2^{CBS} - \frac{A}{X^3} \quad (2)$$

with $X = 3$ and 4, accordingly. We note that the Hartree−Fock energy was not extrapolated separately because it was found to be nearly at the CBS limit for either value of X.

2.2. Description of the Model. Because of the different physical character of the interaction between two water molecules at different separations, the 2B intermolecular potential $V_{2B}(x_a,x_b)$ can be effectively split into short- and long-range contributions

$$V^{(2B)}(x_a, x_b) = V^{(2B)}_{short}(x_a, x_b) + V^{(2B)}_{long}(x_a, x_b) \quad (3)$$

The long-range part is dominated by the (electrostatic) interactions between the permanent and induced moments associated with the molecules' charge distributions and by the dispersion forces. Following the TTM models,[31] the static moments of an isolated water molecule are represented in the MB-pol potential by geometry-dependent point charges derived from the ab initio dipole moment surface calculated by Partridge and Schwenke.[21] As in the TTM2.1-F[19] and TTM4-F[20] models, the point charges are placed on the two hydrogen (H) atoms and on the M site located along the bisector of the HOH angle. The precise position of the M site was chosen to optimize the description of the quadrupole moment of an isolated water molecule. The induction contribution in the MB-pol potential is modeled through a modified version of the Thole-type (TTM) framework employed by the TTM4-F model.[20] Although, as in TTM4-F, the point dipoles are placed on the oxygen (O) and hydrogen (H) atoms, and an increased damping between the intramolecular dipoles on the H atoms is adopted (see Appendix A for a more detailed presentation). Similar to the CC-pol potential,[24] the long-range dispersion contribution is represented by damped r^{-6} and r^{-8} terms associated with all pairs of atoms. The long-range 2B potential is thus approximated as follows

$$V^{(2B)}_{long}(x_a, x_b) = V^{(2B)}_{TTM}(x_a, x_b) + V^{(2B)}_{68}(x_a, x_b) \quad (4)$$

Here, $V^{(2B)}_{TTM} = V^{(2b)}_{TTM,elec} + V^{(2B)}_{TTM,ind}$ and includes Coulomb terms between all charges and induced dipoles (see Appendix A), and

$$V^{(2B)}_{68}(x_a, x_b) = -\sum_{i\in a, j\in b} f_6(\delta_6^{(ij)} r_{ij}) C_6^{(ij)} \frac{1}{r_{ij}^6} - \sum_{i\in a, j\in b} f_8(\delta_8^{(ij)} r_{ij}) C_8^{(ij)} \frac{1}{r_{ij}^8} \quad (5)$$

describes the long-range dispersion interaction. The sums over i and j in eq 5 run over all atoms belonging to molecules a and b, r_{ij} denotes the distance between each pair of atoms, and $f_n(\xi)$ are the Tang−Toennies damping functions[32]

$$f_n(\xi) = 1 - \exp(-\xi) \sum_{k=0}^{n} \frac{\xi^k}{k!} \quad (6)$$

The short-range part of the MB-pol 2B PES (eq 3) is represented in terms of a permutationally invariant polynomial that smoothly switches to zero once the separation between the two water molecules exceeds a predetermined cutoff value

$$V^{(2B)}_{short}(x_a, x_b) = s_2\left(\frac{r_{OO} - R_i}{R_o - R_i}\right) V_{2S} \quad (7)$$

with

$$s_2(x) = \begin{cases} 1 & \text{if } x < 0 \\ 1 + x^2(2x - 3) & \text{if } 0 \le x < 1 \\ 0 & \text{if } 1 \le x \end{cases} \quad (8)$$

The inner and outer radii ($R_{i,o}$) of the switching function are set to 5.5 and 7.5 Å, respectively, providing a good compromise between accuracy and computational efficiency. In eq 7, V_{2S} is a polynomial in functions of the distances between all pairs involving both the physical atoms (H and O) and the two additional sites (L_1 and L_2) located symmetrically along the oxygen lone-pair directions (Figure 1)

$$r_L^{(\pm)} = r_O + \frac{1}{2}\gamma_{\parallel}(r_{OH_1} + r_{OH_2}) \pm \gamma_{\perp}[r_{OH_1} \times r_{OH_2}]$$

Here, $\gamma_{\parallel}$ and $\gamma_{\perp}$ are fitting parameters that determine the optimal location of the L sites, and $\mathbf{r}_{OH_{1,2}}$ are vectors joining the O and H atoms within the same water molecule. All distances,

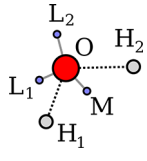

Figure 1. Interaction sites of the MB-pol pair potential.

dx.doi.org/10.1021/ct400863t | J. Chem. Theory Comput. 2013, 9, 5395−5403

$d_{m=1-31}$, appearing in the V_{2S} polynomial are listed in Table 1. Starting from $d_{m=1-31}$, the following variables are formed

Table 1. Distances Entering the Short-Range Part of the Potential[a]

						d_{16}	La1	Hb1
						d_{17}	La1	Hb2
						d_{18}	La2	Hb1
			d_7	Ha1	Hb1	d_{19}	La2	Hb2
d_1	Ha1	Ha2	d_8	Ha1	Hb2	d_{20}	Lb1	Ha1
d_2	Hb1	Hb2	d_9	Ha2	Hb1	d_{21}	Lb1	Ha2
d_3	Oa	Ha1	d_{10}	Ha2	Hb2	d_{22}	Lb2	Ha1
d_4	Oa	Ha2	d_{11}	Oa	Hb1	d_{23}	Lb2	Ha2
d_5	Ob	Hb1	d_{12}	Oa	Hb2	d_{24}	Oa	Lb1
d_6	Ob	Hb2	d_{13}	Ob	Ha1	d_{25}	Oa	Lb2
			d_{14}	Ob	Ha2	d_{26}	Ob	La1
			d_{15}	Oa	Ob	d_{27}	Ob	La2
						d_{28}	La1	Lb1
						d_{29}	La1	Lb2
						d_{30}	La2	Lb1
						d_{31}	La2	Lb2

[a]The first letter of the site label denotes the site name (O, H, or L). The second letter distinguishes the molecules (a or b). The trailing digit indexes the equivalent sites within the molecule.

$$\xi_1 = e^{-k_{HH_{intra}} d_1}$$
$$\cdots$$
$$\xi_6 = e^{-k_{OH_{intra}} d_6}$$
$$\xi_7 = e^{-k_{HH_{coul}} d_7}/d_7$$
$$\cdots$$
$$\xi_{15} = e^{-k_{OO_{coul}} d_{15}}/d_{15}$$
$$\xi_{16} = e^{-k_{LH} d_{16}}$$
$$\cdots$$
$$\xi_{31} = e^{-k_{LL} d_{31}}$$

which are divided into three groups: intramolecular variables (ξ_1,...,ξ_6), intermolecular Coulomb-like variables (ξ_7,...,ξ_{15}), and intermolecular variables involving the L sites (ξ_{16},...,ξ_{31}). On the basis of these definitions, V_{2S} is then constructed as a permutationally invariant polynomial in ξ_i. The invariance is imposed with respect to the permutation of the two water molecules as well as to permutations of equivalent sites (O, H_1, H_2, L_1, and L_2) within each molecule. The following symmetrized monomials are included in V_{2S}: (a) six first-degree monomials formed from all intermolecular (ξ_7,...,ξ_{31}) variables,

$$\eta_1 = \sum_{i=16}^{23} \xi_i$$
$$\eta_2 = \xi_{28} + \xi_{29} + \xi_{30} + \xi_{31}$$
$$\eta_3 = \xi_{15}$$
$$\cdots$$

(b) 63 second-degree symmetrized monomials with at most linear intramolecular terms, (c) 491 symmetrized third-degree monomials with at most a quadratic dependence on the intramolecular variables, and (d) 593 fourth-degree terms quadratic with respect to the intramolecular variables. The complete list of all 1153 symmetrized monomials entering $V_{2S} = \sum_{l=1}^{1153} c_l \eta_l$ is available in the Supporting Information. The coefficients c_l along with $C_{6,8}^{(HH)}$, $C_{6,8}^{(OH)}$, and $C_{6,8}^{(OO)}$ are linear fitting parameters. $V_2(x_a,x_b)$ in eq 3 also includes 16 nonlinear parameters: $\delta_{6,8}^{(HH)}$, $\delta_{6,8}^{(OH)}$, $\delta_{6,8}^{(OO)}$, $\gamma_\perp$, $\gamma_\parallel$, $k_{HH_{intra}}$, $k_{OH_{intra}}$, $k_{HH_{coul}}$, $k_{OH_{coul}}$, $k_{OO_{coul}}$, k_{LH}, k_{LO}, and k_{LL}.

2.3. Fitting. Following the CC-pol strategy,[24] the fitting process of the 2B MB-pol parameters was carried out in two stages. The $C_{6,8}^{(ab)}$ were first obtained with $\delta_{6,8}^{(ab)}$ set to infinity (i.e., without the Tang−Toennies damping). The long-range training set comprised one million dimers formed from randomly oriented molecules in the vibrationally averaged geometry (r_{OH} = 1.836106337 Bohr and ϑ_{HOH} = 104.69° as defined in ref 24). The distances between the monomer centers of mass were sampled uniformly from 9 to 21 Bohr. [The asymptotic long-range energy becomes inaccurate for COM−COM separations below 9 Bohr, and the energies become vanishingly small above 21 Bohr.] The sum of the $C_6^{(ab)}$ values was fixed[24] to ensure the correct long-range behavior

$$C_6^{(OO)} + 4C_6^{(OH)} + 4C_6^{(HH)} + 2\alpha\mu^2 = C_6^{ref} \quad (9)$$

Here, the last term in the left-hand side represents the isotropic contribution due to the Coulomb interaction between the permanent dipole of one monomer and the induced dipole of the other monomer. Assuming vibrationally averaged monomer geometries, the values of the isotropic polarizability (α = 1.43016 Å^3) and the molecular dipole (μ = 1.8679D) were taken from the TTM model and Partridge−Schwenke dipole moment surface. The reference value (C_6^{ref} = 57.718405 au) on the right-hand side of eq 9 was computed from "first principles" in ref 24. The $C_{6,8}$ values obtained from the least-squares fit are reported in the Supporting Information.

After determining $C_{6,8}^{(ab)}$, the coefficients of the short-range polynomial ($c_{l=1,...,1153}$) along with the 16 nonlinear parameters were obtained by minimizing the (regularized) weighted sum of squared residuals calculated for the short-range training set $\mathcal{S}$(42508 dimers)

$$\chi^2 = \sum_{n\in\mathcal{S}} w_n [V_2^{model}(n) - V_2^{ref}(n)]^2 + \Gamma^2 \sum_{l=1}^{1153} c_l^2$$

The weights, w_n, were set to emphasize dimers with lower total energy

$$w(E) = \left(\frac{\Delta E}{E - E_{min} + \Delta E}\right)^2 \quad (10)$$

Here, E_{min} denotes the lowest energy in the training set (i.e., dimer global minimum energy), and ΔE defines the range of favorably weighted energies, which was set to 25 kcal/mol upon careful experimentation. The regularization parameter, Γ, was set to 5×10^{-4} in order to reduce the variation of the linear fitting parameters (larger Γ values effectively suppress any variation) without spoiling the overall accuracy of the fit (favored by smaller Γ values), contributing no more than 1% to χ^2. The linear parameters ($c_{l=1,...,1153}$) were obtained through singular value decomposition, while the simplex algorithm was used to optimize the nonlinear parameters. The optimal value of χ^2 was 54.79 (kcal/mol)^2, corresponding to an RMS error of 0.054 kcal/mol per dimer. The RMS error over the lowest 25 kcal/mol was 0.00077 kcal/mol and the largest error over the

dx.doi.org/10.1021/ct400863t | J. Chem. Theory Comput. 2013, 9, 5395−5403

lowest 25 kcal/mol was 0.67 kcal/mol. The optimal values of all parameters are listed in the Supporting Information along with the correlation plots illustrating the accuracy of the CCpol-8s/f, HBB2, and MB-pol potentials.

2.4. Short-Range Training Set. The short-range training set used in the fitting process contained 42508 dimers with COM−COM separations ranging from 1.6 to 8 Å. Specifically, the training set included (a) the same training set used in ref 24 for the development of the rigid version of the CC-pol model, (b) dimers extracted from path−integral molecular dynamics (PIMD) simulations of liquid water at ambient temperature and experimental density carried out with the HBB2-pol potential,[33] and (c) the dimer global minimum structure and the nine saddle points along with representative configurations located in their neighborhoods. A larger ensemble of configurations was first formed for (b) and (c), containing approximately an order of magnitude more dimers than actually used in the final fitting process. These initial configurations were then "strained", and only dissimilar geometries as determined from an RMSD criterion were kept in the final ensemble .

It is important to note that in principle a systematic "gridding" would have provided the perfect training set, uniformly representing the relevant regions of the configurational space. Unfortunately, given the dimensionality of the problem, this procedure cannot be performed for flexible water dimer configurations. However, we believe that dimer structures extracted from both PIMD trajectories and neighborhoods of the stationary points are sufficiently representative of the energy range relevant to molecular simulations of water under conditions of moderate temperature and pressure. In addition, within the protocol described above, the geometric uniformity of the training set is approximately achieved via the "straining" step. The training set geometries, along with the reference energies, are reported in the Supporting Information.

3. VALIDATION

3.1. Stationary Points. The total energies and corresponding gradients calculated at the 10 stationary points of the ab initio water dimer PES reported in ref 34 are listed in Table 2. The same quantities for geometries optimized on the MB-pol PES are given in Table 3 along with the RMS values calculated relative to the ab initio configurations of ref 34. Both sets of results clearly demonstrate the good agreement between the MB-pol and ab initio PESs.

Table 2. Energies for Reference Saddle Point Geometries[a]

no.	E (cm^{-1})	$\lvert\nabla E\rvert_2$ (Eh/Bohr)	ΔE (cm^{-1})	ΔE (cm^{-1}) [ref]
1	−1732.02	7.98e-04	0.00	0.00
2	−1555.58	8.22e-04	176.44	181.00
3	−1536.01	7.92e-04	196.01	198.00
4	−1497.30	7.14e-04	234.72	245.00
5	−1416.28	8.20e-04	315.74	333.00
6	−1399.35	8.70e-04	332.67	348.00
7	−1108.00	7.08e-04	624.02	634.00
8	−493.60	7.41e-04	1238.42	1249.00
9	−1109.34	6.78e-04	622.68	625.00
10	−797.04	7.42e-04	934.98	948.00

[a]RMS error is 10.8 cm^{-1}.

Table 3. Energies for Optimized Saddle Point Geometries[a]

no.	E (cm^{-1})	$\lvert\nabla E\rvert_2$ (Eh/Bohr)	RMS (Å)	ΔE (cm^{-1})	ΔE (cm^{-1}) [ref]
1	−1734.74	1.16e-10	6.95e-03	0.00	0.00
2	−1557.04	1.49e-10	1.71e-02	177.70	181.00
3	−1538.19	2.01e-10	5.32e-03	196.55	198.00
4	−1499.53	6.87e-11	5.89e-03	235.21	245.00
5	−1419.30	1.76e-10	7.80e-03	315.43	333.00
6	−1402.28	1.33e-10	3.37e-03	332.46	348.00
7	−1104.09	1.43e-10	5.22e-02	630.65	634.00
8	−495.54	4.40e-11	7.06e-03	1239.20	1249.00
9	−1110.98	1.33e-10	4.37e-03	623.75	625.00
10	−799.41	7.29e-11	1.16e-02	935.33	948.00

[a]RMS error is 10.2 cm^{-1}.

The accuracy of the potential is further illustrated in Figure 2 showing the comparison between the MB-pol and CCSD(T)/CBS interaction energies for optimized configurations of the water dimer at different O−O separations with the optimization carried out on the WHBB PES. Because these configurations, with the exception of the global minimum energy structure, were not included in the short-range training set, the level of agreement with the ab initio data provides evidence for the overall high accuracy of the MB-pol PES.

3.2. VRT Spectrum. The $(H_2O)_2$ VRT spectrum was calculated using the [6 + 6]-dimensional ([6 + 6]D) adiabatic decoupling method developed by Leforestier and co-workers.[35] Although approximate, this method is sufficiently accurate for the water dimer and was used to calculate the $(H_2O)_2$ VRT spectrum with the CC-pol[36] and HBB2[37] potentials. The results given below were obtained using the same basis specifications as in these two papers. Because a detailed description of the methodology used for the calculation of the VRT spectrum has already been reported in the literature,[36,37] only the computational details specific to the present study are given here.

In Table 4, we report the energy levels, i.e., the origins $o_1(K)$ and $o_2(K)$ for $K = 0$ and $K = 1$, and corresponding interchange tunneling splittings $i_1(K)$ and $i_2(K)$, calculated with the 2B MB-pol potential. Also listed are the corresponding experimental data and the results obtained with the CCpol-8s/f[36] and HBB2[37] potentials.

Following ref 36, indices (1) and (2) refer to the $(A_1^{\pm}, B_1^{\pm})$ and $(A_2^{\pm}, B_2^{\pm})$ subforks, respectively, which are associated with each value of the projection quantum number K. Here, $A_1^{\pm}$, $B_1^{\pm}$, $A_2^{\pm}$, and $B_2^{\pm}$ identify one-dimensional irreducible representations of the molecular symmetry group G_{16} of the water dimer (see ref 35 for a detailed description). The splittings between the (1) and (2) levels are due to acceptor tunneling. Because the water dimer can be classified as a nearly prolate symmetric top, the origins o_1 and o_2 of the subforks are usually defined using the following expression

$$E_i(J, K) = o_i(K) + \frac{B + C}{2}[J(J + 1) - K^2] \quad (11)$$

where J is the total dimer angular momentum quantum number, and $E_i(J,K)$ corresponds to the average energy of the $A_i^{\pm}$ and $B_i^{\pm}$ levels belonging to each subfork. The origin $o_i(K = 0)$ is set to zero, so that all other $o_i(K)$ values can effectively be considered as excitation energies. The values given in parentheses in Table 4 correspond to the splittings $i_i(K) = |A_i^{\pm} - B_i^{\pm}|$ between levels within each subfork that arise from the

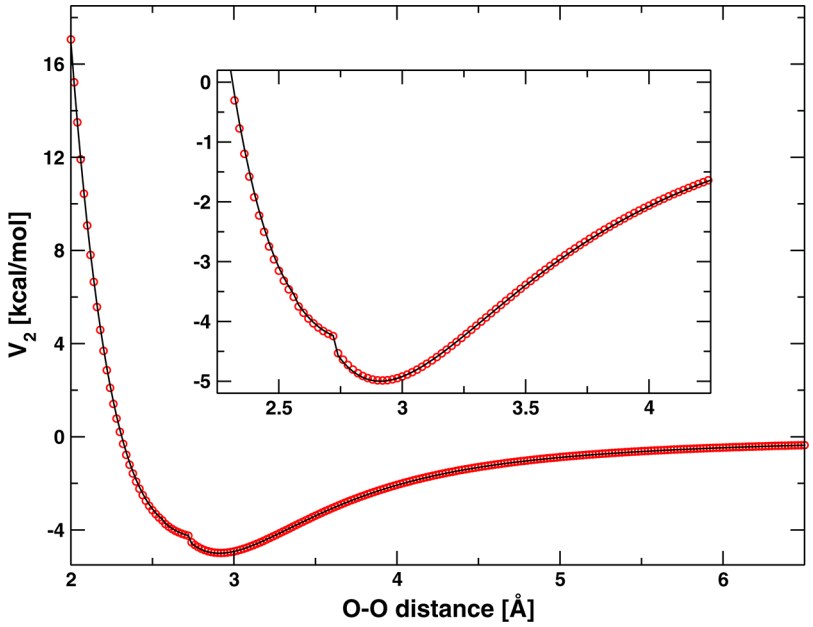

Figure 2. Intermolecular interaction energy for the water dimer geometries optimized at the fixed values of the oxygen−oxygen separations on the WHBB PES: MB-pol (solid line), CCSD(T)/CBS (red circles).

Table 4. Experimental[38−42] and Calculated VRT Levels and Tunneling Splittings of (H_2O_2)[a]

			experiment	HBB2	CCpol-8s/f	MB-pol		experiment	HBB2	CCpol-8s/f	MB-pol
OO	—	(2)	153.62(1.88)	148.57(1.14)	149.63(1.23)	154.31(2.41)	(1)		152.50(1.12)	152.07(1.48)	156.60(2.71)
	—	(1)		145.00(3.48)	143.20(3.27)	149.44(1.97)	(2)		150.52(1.04)	153.54(2.54)	152.69(4.13)
AT	—	(1)		128.91(0.74)	132.10(1.48)	129.44(0.24)	(1)		142.25(4.33)	142.42(4.04)	143.68(4.87)
	—	(2)	120.19(9.39)	121.01(8.41)	117.50(8.67)	119.07(10.15)	(2)		136.24(5.31)	136.52(4.66)	137.04(5.95)
AW	—	(2)	108.89(0.02)	105.78(0.03)	107.82(0.10)	108.87(0.13)	(2)	123.56(3.41)	122.25(2.48)	123.12(3.16)	123.65(3.83)
	—	(1)	107.93(2.95)	105.35(1.99)	109.23(3.29)	108.38(3.24)	(1)	109.98(5.24)	108.95(4.55)	108.28(4.76)	109.65(5.89)
DT	—	(1)		116.54(4.84)	113.35(5.91)	113.83(5.61)	(2)		94.25(2.66)	92.18(3.34)	91.22(3.47)
	—	(2)	64.52(2.54)	67.18(2.03)	61.33(2.48)	61.31(2.54)	(1)	87.75(1.11)	89.55(0.54)	86.37(1.32)	85.63(1.00)
GS	—	(2)	11.18(0.65)	10.16(0.60)	12.75(0.61)	12.05(0.69)	(1)	14.39(0.70)	14.00(0.64)	15.45(0.67)	15.04(0.77)
	—	(1)	0.00(0.75)	0.00(0.68)	0.00(0.72)	0.00(0.81)	(2)	11.66(0.54)	11.50(0.49)	12.36(0.51)	12.18(0.48)
				$K = 0$					$K = 1$		

[a]Ground state (GS), donor torsion (DT), acceptor wag (AW), acceptor twist (AT), and intermolecular stretch (OO). The energies (cm^{-1}) correspond to the origins $o_1(K)$ and $o_2(K)$ of the levels (1) and (2) with quantum numbers $K = 0$ and $K = 1$, respectively. The values in parentheses are the interchange tunneling splittings $i_1(K)$ and $i_2(K)$ defined in the text. The values for CCpol-8sf and HBB2 are taken from refs 36 and 37 correspondingly.

donor−acceptor interchange tunneling. The acceptor tunneling splitting $a_i(K)$ between the subforks (1) and (2) is instead defined as $|o_1(K) - o_2(K)|$. Overall the VRT spectrum calculated with the MB-pol potential is in very good agreement with the corresponding experimental results, which is comparable to, if not slightly better than, that provided by the CCpol-8s/f and HBB2 potentials.

The frequency shift of each monomer vibration was also calculated by subtracting the energy of the dimer ground-state level computed on the lowest adiabatic 6D potential (with both monomers in their ground state) from the dimer ground-state level computed on the excited adiabatic potential obtained for the corresponding monomer vibration. Table 5 shows that the frequency shifts predicted with the MB-pol potential are in very good agreement with the available experimental data and of similar accuracy of those reported in the literature for the CCpol-8s/f and HBB2 potentials. In this regard, it should be noted that a direct comparison with the experimental data is not completely straightforward because the latter were obtained from very different sources, including high-resolution molecular beam IR spectra only for the $as[A]$ mode, cavity ringdown spectra only for the bend modes, size-selected cluster molecular

Table 5. Infrared Shifts of Water Dimer Excitation Frequencies (cm^{-1})[a]

mode	experiment	MB-pol	CCpol-8s/f	HBB2
$b[D]$	+20[b]	14.2	+13.4	+17.1
$O-H_b[D]$	−56[c], −59.0[d]	−54.6	−61.6	−44.8
$O-H_f[D]$	−21[c], −25.3, and −26.3[d]	−22.0	−13.5	−22.3
$b[A]$	+6[b]	+5.9	+7.3	+7.2
$ss[A]$	−2.2[d] (−2 to +3[e])	−3.4	−7.1	−1.7
$as[A]$	−11[f]	−6.7	−6.6	−5.7

[a]$b[D]$, donor bending; $O-H_b[D]$ and $O-H_f[D]$, two donor OH stretches; $b[A]$, acceptor bending; ss $[A]$, acceptor symmetric stretch; as $[A]$, acceptor antisymmetric stretch. Results for the CCpol-8s/f and HBB2 potentials are from refs 36 and 37, correspondingly. [b]From cavity ringdown spectra (ref 43). [c]From size-selected cluster molecular beam spectra (refs 44 45). [d]From helium droplet spectra (ref 46). [e]Extrapolated value from solid noble gas matrix spectra (refs 47 48). [f]From ref 49.

dx.doi.org/10.1021/ct400863t | J. Chem. Theory Comput. 2013, 9, 5395−5403

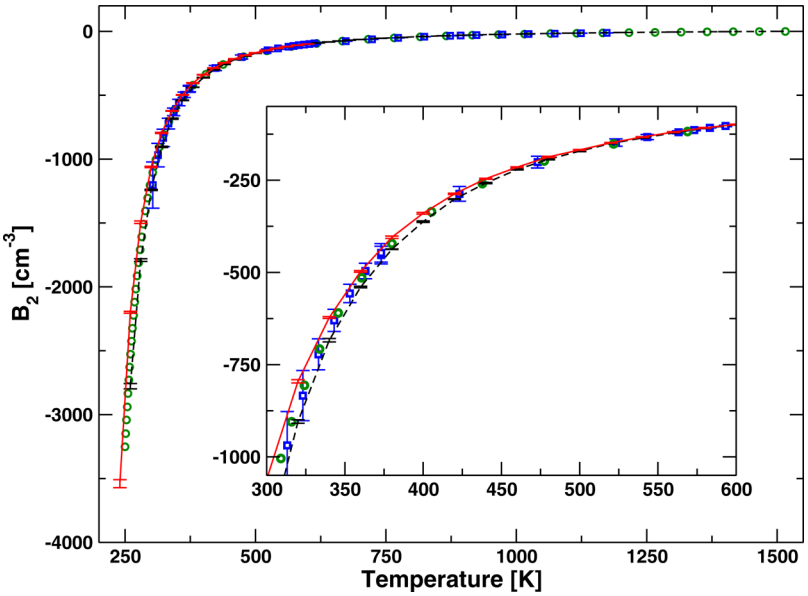

Figure 3. Second virial coefficient computed using classical (dashed line) and quantum (solid line) description of the water molecules. The experimental data from refs 50 and 51 are shown as circles and squares, respectively. (The data from ref 50 are obtained from a fit to the experimental results; please see the original reference for a discussion on the corresponding uncertainties).

beam spectra, matrix spectra in solid noble gas matrices, and spectra in low-temperature helium nanodroplets for all the O−H stretch modes. As discussed in ref 36, in the lower resolution spectra, the bands are quite broad and not resolved, so it is not clear which of the calculated tunneling components and rotational transitions actually correspond to the frequency shifts extracted from these spectra. In matrix spectra, the frequencies are shifted by an unknown amount due to the effect of the surrounding matrix, although such shifts are probably small in the case of helium nanodroplets.

3.3. Second Virial Coefficient. The second virial coefficient, $B_2(T)$, for flexible water molecules is given by

$$B_2(T) = -2\pi \int dR_{ab} R_{ab}^2 \left\langle f_{ab} \right\rangle_{\Omega_a,\Omega_b,\boldsymbol{\nu}_a,\boldsymbol{\nu}_b} \tag{12}$$

where $f_{ab} = e^{-\beta V_{2B}(x_a,x_b)}$, R_{ab} is the distance between the molecules' centers of mass, and the angular brackets denote the average over the orientations and geometries of both monomers. In the classical case, the latter obey the Boltzmann distribution

$$\langle f_{ab} \rangle_{\Omega_a,\Omega_b,\boldsymbol{\nu}_a,\boldsymbol{\nu}_b} = \frac{\int d\Omega_a d\Omega_b d\boldsymbol{\nu}_a d\boldsymbol{\nu}_b e^{-\beta V(a)} e^{-\beta V(b)} f_{ab}}{\left(\int d\boldsymbol{\nu}_a e^{-\beta V(a)}\right)\left(\int d\Omega_a\right)\left(\int d\boldsymbol{\nu}_a e^{-\beta V(a)}\right)\left(\int d\Omega_a\right)} \tag{13}$$

Extension to the quantum case is achieved through the path-integral formalism in which the averages over $\boldsymbol{\nu}_{a,b}$ are performed by the corresponding path integrals and the intermolecular interaction $V_{2B}(x_a,x_b)$ is replaced by its (quantum) mean value over the monomers' paths. To evaluate eq 12, the angular and thermal averages of the Mayer function were first calculated on a grid of monomers' COM−COM separations spanning the 2.2 Å < R < 25 Å range using 1024 points. These averages were performed through Monte Carlo integration using 10^6 samples at each radial R grid point. To this end, thermally distributed monomer (or corresponding ring polymers in the quantum case) configurations were generated from both classical and path-integral molecular dynamics simulations of isolated molecules that were subsequently put in random orientations with respect to each other. The radial integration was then performed using Simpson's rule, and the statistical uncertainties were estimated from the results for 10 blocks for 10^5 samples each. In the PIMD simulations, the Feynman path integrals were discretized using 32 beads. Both classical (black dashed line) and quantum (red solid line) results for B_2 are shown in Figure 3 along with the available experimental data. As expected, larger deviations between classical and quantum behaviors are found at lower temperature, with the two sets of calculated values becoming effectively indistinguishable above T = 450 K. Interestingly, both classical and quantum results are within the experimental uncertainties, providing further evidence of the overall accuracy of the MB-pol potential for the water dimer.

4. SUMMARY

In this study, we have described the development of the two-body term (V_{2B}) of a new water potential with flexible monomers (MB-pol) derived entirely from "first principles". V_{2B} represents the full-dimensional intermolecular part of the water dimer potential energy surface. Within the MB-pol scheme, V_{2B} is constructed as the combination of an invariant polynomial at short-range and a "first principles" description of the interaction energy at long-range, with induction contributions present at all intermolecular separations. The parameters entering the functional form of V_{2B} were determined by fitting 40,000 dimer energies calculated at the CCSD(T)/CBS level of theory and imposing the correct asymptotic behavior at long-range as predicted from "first principles". We have shown that very good agreement is obtained between the vibration−rotation tunneling (VRT) spectrum of the water dimer calculated with the MB-pol V_{2B} potential using a [6 + 6]D adiabatic decoupling method and the corresponding experimental results. The level of agreement between MB-pol and

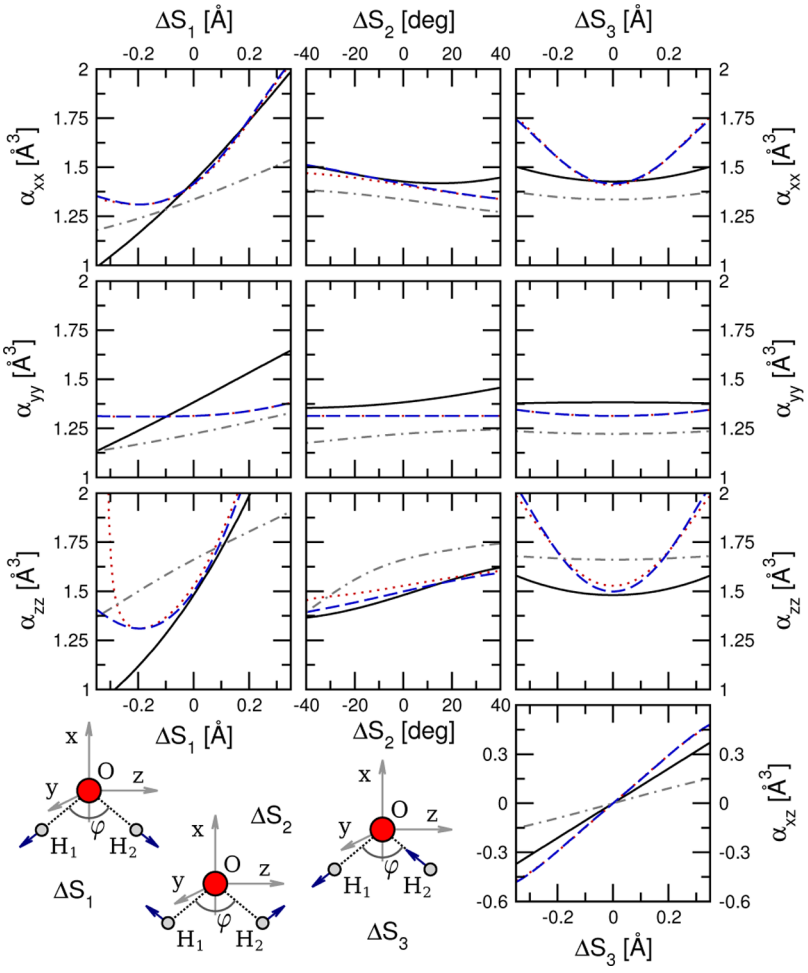

Figure 4. Nonzero components of the molecular dipole polarizability tensor (rows) for isolated water molecule in the geometries obtained by deforming the molecule along the symmetric stretch (left column), bend (middle column), and asymmetric stretch (right column). The molecule is in the *xz* plane with the *x* axis bisecting the H−O−H angle. Solid line, CCSD(T); dotted line, TTM4-F; dashed line, MB-pol; and dashed−dotted line, AMOEBA.

experimental spectra is comparable to, if not slightly better than, that reported in the literature for calculations carried out with the CCpol-8s/f and HBB2 potentials. The second virial coefficient calculated as a function of temperature at both classical and quantum levels with the MB-pol potential is also found in good agreement with the available experimental data, providing further evidence for the accuracy of V_{2B}. In forthcoming studies, we will describe the development and implementation of many-body energy contributions within the MB-pol potential and will report on molecular simulations for both water clusters and condensed-phase systems, which will be discussed in the context of other machine-learning-based approaches.[56]

APPENDIX

A. Thole-Type Electrostatics Model

A slightly re-parameterized variant of the Thole-type model version 4 (TTM4-F[20]) is utilized by MB-pol for the description of electrostatic interactions. The Thole-type models, built upon the Applequist[52] and Thole[53] ideas, mimic the electronic polarization effects by introducing inducible point dipoles whose magnitude is proportional to the electric field created by both the point charges and the inducible dipoles themselves. Consequently, the latter must be solved for self-consistently. To avoid over-polarization, Coulomb interactions between the point objects (charges and dipoles in our case) are softened at small distances via smearing of the corresponding charge densities over some volume. The electrostatic (TTM) part of the energy reads[20]

$$V_{\mathrm{TTM}} = V_{\mathrm{CC}} + V_{\mathrm{CD}} + V_{\mathrm{DD}} + V_{\mathrm{spring}}$$

where V_{CC}, V_{CD}, and V_{DD} denote the charge−charge, charge-dipole, and dipole−dipole contributions

$$V_{\mathrm{CC}} = \frac{1}{2}\sum_{a\neq b} q_a q_b A_{ab}^{-1}\lambda_1(u_{ab})$$

$$V_{\mathrm{CD}} = \sum_{a\neq b} q_a(\boldsymbol{\mu}_b\cdot\boldsymbol{r}_{ab})A_{ab}^{-3}\lambda_3(u_{ab})$$

$$V_{\mathrm{DD}} = \frac{1}{2}\sum_{a\neq b}[(\boldsymbol{\mu}_a\cdot\boldsymbol{\mu}_b)A_{ab}^{-3}\lambda_3(u_{ab}) - 3(\boldsymbol{\mu}_a\cdot r_{ab})(\boldsymbol{\mu}_b\cdot\boldsymbol{r}_{ab})A_{ab}^{-5}\lambda_5(u_{ab})]$$

and V_{spring} is

$$V_{\mathrm{spring}} = \frac{1}{2}\sum_{a}\frac{1}{\alpha_a}(\boldsymbol{\mu}_a\cdot\boldsymbol{\mu}_a)$$

dx.doi.org/10.1021/ct400863t | J. Chem. Theory Comput. 2013, 9, 5395−5403

The $\boldsymbol{r}_{ab}$ in the equations above is the vector joining the interaction sites a and b ($\boldsymbol{r}_{ab} = \boldsymbol{r}_a - \boldsymbol{r}_b$), q_a and $\boldsymbol{\mu}_a$ are the charges and induced dipoles correspondingly, $u_{ab} = r_{ab}/A_{ab}$, $A_{ab} = (\alpha_a\alpha_b)^{1/6}$, and α_n are the dipole polarizabilities. Functions $\lambda_n(u)$ implement the screened interactions by assuming a particular density in place of the point charges.

$$\lambda_{n+2}(u) = -\frac{1}{un}\frac{\partial}{\partial u}\lambda_n(u)$$

$$\lambda_1(u) = \frac{1}{u}(1 - \mathrm{e}^{-au^m}) + a^{1/m}\Gamma\left[1 - \frac{1}{m}, au^m\right]$$

$$\lambda_3(u) = \frac{1}{u^3}(1 - \mathrm{e}^{-au^m})$$

$$\lambda_5(u) = \frac{1}{u^2}\lambda_3(u) - \frac{am}{3}u^{m-5}\mathrm{e}^{-au^m}$$

$$\Gamma(a, x) = \int_x^\infty \mathrm{d}t t^{a-1}\mathrm{e}^{-t}$$

The value of m is set to 4 in the TTM4-F model.

For the given positions of the interaction sites, the induced dipoles, $\boldsymbol{\mu}_a$, must minimize V_{TTM}

$$\frac{\partial}{\partial \boldsymbol{\mu}_a}V_{\mathrm{TTM}} = 0$$

With these (actual) values of $\boldsymbol{\mu}$, the energy function simplifies to the following form

$$V_{\mathrm{TTM}} = V_{\mathrm{TTM,elec}} + V_{\mathrm{TTM,ind}}$$

$$V_{\mathrm{TTM,elec}} = V_{\mathrm{CC}}$$

$$V_{\mathrm{TTM,ind}} = -\frac{1}{2}\sum_a (\boldsymbol{\mu}_a \cdot \boldsymbol{E}_a)$$

where $\boldsymbol{E}_a$ denotes the (attenuated via the Thole smearing) electric field at the a-th interaction site due to the charges and dipoles.

The model utilizes three geometry-dependent point charges derived from the Partridge–Schwenke[21] DMS. Two positive charges are placed at the hydrogen atoms, while the negative charge is shifted from the oxygen atom to the so-called M site in order to approximate the quadrupole moment of the isolated water molecule better. There are also three polarizable sites per molecule located at the atoms with the intra-molecular charge–charge and charge–dipole interactions assumed to be zero (excluded). The dipole–dipole intra-molecular contributions are allowed effectively encoding the dependence of the molecular polarizability on the molecular geometry. There is six parameters in the original TTM4-F model:[20] two polarizabilities ($\alpha_{\mathrm{H}} = 0.294$ Å^3, $\alpha_{\mathrm{O}} = 1.31$ Å^3) and four damping factors $a_{\mathrm{CC}} = 0.4$, $a_{\mathrm{CD}} = 0.4$, $a_{\mathrm{DD,inter}} = 0.055$, and $a_{\mathrm{DD,intra}} = 0.626$. It turned out that the original model is unstable for some deformed monomer geometries that do occur (albeit not too often) in PIMD simulations of small clusters as well as condensed phases at ambient conditions. The instability is due to the insufficient damping of the 1–3 (hydrogen–hydrogen) intra-molecular dipole–dipole interactions. It has been found that the (good) properties of the model are largely unaffected by the changes of the corresponding $a_{\mathrm{DD,intra}}$ parameter, so its value for MB-pol has been set to 0.055 (as used for the inter-molecular dipole–dipole interactions). To illustrate the performance of the model, the molecular polarizability of isolated water molecule is shown in the Figure 4 for the distorted molecular geometries. The first-principles data from ref 54 are also shown along with the values predicted by the popular AMOEBA[55] force field. The magnitudes of the distortions are defined as follows

$$\Delta S_1 = (\Delta R_1 + \Delta R_2)/\sqrt{2}$$

$$\Delta S_2 = \Delta\phi$$

$$\Delta S_3 = (\Delta R_2 - \Delta R_1)/\sqrt{2}$$

where $\Delta R_{1,2}$ and $\Delta\varphi$ denote the O–H distances and the H–O–H angle with respect to the reference geometry $R^0_{1,2} = 0.95843$ Å and $\phi^0 = 104.44°$ as assumed in ref 54. The instability of the original TTM4-F model is clearly visible in the behavior of the α_{zz} component of the polarizability tensor for the symmetrically stretched configurations. The plots also show that the adjustments to the intra-molecular dipole–dipole damping indeed had a very minor effect on the overall quality of the model. Neither TTM4-F nor AMOEBA is able to reproduce the molecular polarizability, yet the former model does a much better job capturing many-body interactions of water molecules.[17]

■ ASSOCIATED CONTENT

Ⓢ Supporting Information

Tranining set used for the short-range two-body part of the MB-pol potential. List of the monomials contributing to V_{2S}. Reference implementation of the potential. Comparison of CCpol-8sf, HBB2, and MB-pol against CCSD(T)/CBS energies. This material is available free of charge via the Internet at http://pubs.acs.org.

■ AUTHOR INFORMATION

Corresponding Authors

*E-mail: vbabin@ucsd.edu (V.B.).
*E-mail: Claude.Leforestier@univ-montp2.fr (C.L.).
*E-mail: fpaesani@ucsd.edu (F.P.).

Notes

The authors declare no competing financial interest.

■ ACKNOWLEDGMENTS

This research was supported by the National Science Foundation through Grant CHE-1111364 and by the Agence Nationale de la Recherche Grant ANR-12-BS08-0010-01. We are grateful to the National Science Foundation for a generous allocation of computing time on Xsede resources (Award TG-CHE110009). Additionally, we thank Greg Medders for his valuable feedback in preparation of this manuscript.

■ REFERENCES

(1) Chalasinski, G.; Szczesniak, M. M. *Chem. Rev.* **2000**, *100*, 4227–4252.
(2) Molinero, V.; Moore, E. B. *J. Phys. Chem. B* **2009**, *113*, 4008–4016.
(3) Vega, C.; Abascal, J. L. F. *Phys. Chem. Chem. Phys.* **2011**, *13*, 19663–19688.
(4) Dang, L. X.; Pettitt, B. M. *J. Phys. Chem.* **1987**, *91*, 3349–3354.
(5) Fanourgakis, G. S.; Xantheas, S. S. *J. Chem. Phys.* **2008**, *128*, 074506.
(6) Lee, A. J.; Rick, S. W. *J. Chem. Phys.* **2011**, *134*, 184507.
(7) Wernet, P.; Nordlund, D.; Bergmann, U.; Cavalleri, M.; Odelius, M.; Ogasawara, H.; Nöslund, L. Å.; Hirsch, T. K.; Ojamë, L.; Glatzel, P.; Pettersson, L. G. M.; Nilsson, A. *Science* **2004**, *304*, 995–999.

(8) Clark, G. N.; Cappa, C. D.; Smith, J. D.; Saykally, R. J.; Head-Gordon, T. *Mol. Phys.* **2010**, *108*, 1415−1433.
(9) Pieniazek, P. A.; Tainter, C. J.; Skinner, J. L. *J. Am. Chem. Soc.* **2011**, *133*, 10360−10363.
(10) Nihonyanagi, S.; Ishiyama, T.; Lee, T.-k.; Yamaguchi, S.; Bonn, M.; Morita, A.; Tahara, T. *J. Am. Chem. Soc.* **2011**, *133*, 16875−16880.
(11) Kumar, P.; Franzese, G.; Stanley, H. E. *J. Phys.: Condens. Matter* **2008**, *20*, 244114.
(12) Limmer, D. T.; Chandler, D. *J. Chem. Phys.* **2011**, *135*, 134503.
(13) Limmer, D. T.; Chandler, D. *J. Chem. Phys.* **2013**, *138*, 214504.
(14) Jorgensen, W. L.; Tirado-Rives, J. *Proc. Natl. Acad. Sci. U.S.A.* **2005**, *102*, 6665−6670.
(15) Bukowski, R.; Szalewicz, K.; Groenenboom, G. C.; van der Avoird, A. *Science* **2007**, *315*, 1249−1252.
(16) Wang, Y.; Huang, X.; Shepler, B. C.; Braams, B. J.; Bowman, J. M. *J. Chem. Phys.* **2011**, *134*, 094509.
(17) Medders, G. R.; Babin, V.; Paesani, F. *J. Chem. Theory Comput.* **2013**, *9*, 1103−1114.
(18) Mayer, J. E.; Mayer, M. G. *Statistical Mechanics*; John Wiley & Sons Inc: New York, 1940.
(19) Fanourgakis, G. S.; Xantheas, S. S. *J. Phys. Chem. A* **2006**, *110*, 4100−4106.
(20) Burnham, C. J.; Anick, D. J.; Mankoo, P. K.; Reiter, G. F. *J. Chem. Phys.* **2008**, *128*, 154519.
(21) Partridge, H.; Schwenke, D. W. *J. Chem. Phys.* **1997**, *106*, 4618−4639.
(22) Ahlrichs, R. *Theor. Chim. Acta* **1976**, *41*, 7−15.
(23) Rijks, W.; Wormer, P. E. S. *J. Chem. Phys.* **1989**, *90*, 6507−6519.
(24) Bukowski, R.; Szalewicz, K.; Groenenboom, G. C.; van der Avoird, A. *J. Chem. Phys.* **2008**, *128*, 094314.
(25) Werner, H.-J.; Knowles, P. J.; Knizia, G.; Manby, F. R.; Schütz, M.; Celani, P.; Korona, T.; Lindh, R.; Mitrushenkov, A.; Rauhut, G.; Shamasundar, K. R.; Adler, T. B.; Amos, R. D.; Bernhardsson, A.; Berning, A.; Cooper, D. L.; Deegan, M. J. O.; Dobbyn, A. J.; Eckert, F.; Goll, E.; Hampel, C.; Hesselmann, A.; Hetzer, G.; Hrenar, T.; Jansen, G.; Köppl, C.; Liu, Y.; Lloyd, A. W.; Mata, R. A.; May, A. J.; McNicholas, S. J.; Meyer, W.; Mura, M. E.; Nicklass, A.; O'Neill, D. P.; Palmieri, P.; Peng, D.; Pflüger, K.; Pitzer, R.; Reiher, M.; Shiozaki, T.; Stoll, H.; Stone, A. J.; Tarroni, R.; Thorsteinsson, T.; Wang, M. *MOLPRO*, version 2012.1, a package of ab initio programs, 2012; see http://www.molpro.net.
(26) Boys, S.; Bernardi, F. *Mol. Phys.* **1970**, *19*, 553−566.
(27) Dunning, T. H. *J. Chem. Phys.* **1989**, *90*, 1007−1023.
(28) Tao, F.-M.; Pan, Y.-K. *J. Chem. Phys.* **1992**, *97*, 4989−4995.
(29) Halkier, A.; Klopper, W.; Helgaker, T.; Jørgensen, P.; Taylor, P. R. *J. Chem. Phys.* **1999**, *111*, 9157−9167.
(30) Halkier, A.; Helgaker, T.; Jørgensen, P.; Klopper, W.; Olsen, J. *Chem. Phys. Lett.* **1999**, *302*, 437−446.
(31) Burnham, C. J.; Xantheas, S. S. *J. Chem. Phys.* **2002**, *116*, 5115−5124.
(32) Tang, K. T.; Toennies, J. P. *J. Chem. Phys.* **1984**, *80*, 3726−3741.
(33) Babin, V.; Medders, G. R.; Paesani, F. *J. Phys. Chem. Lett.* **2012**, *3*, 3765−3769.
(34) Tschumper, G. S.; Leininger, M. L.; Hoffman, B. C.; Valeev, E. F.; Quack, M.; Schaffer, H. F., III *J. Chem. Phys.* **2002**, *116*, 690−701.
(35) Leforestier, C.; Gatti, F.; Fellers, R. S.; Saykally, R. J. *J. Chem. Phys.* **2002**, *117*, 8710−8722.
(36) Leforestier, C.; Szalewicz, K.; van der Avoird, A. *J. Chem. Phys.* **2012**, *137*, 014305.
(37) Leforestier, C. *Philos. Trans. R. Soc., A* **2012**, *370*, 2675−2690.
(38) Braly, L. B.; Liu, K.; Brown, M. G.; Keutsch, F. N.; Fellers, R. S.; Saykally, R. J. *J. Chem. Phys.* **2000**, *112*, 10314−10326.
(39) Keutsh, F. N.; Goldman, N.; Harker, H. A.; Leforestier, C.; Saykally, R. J. *Mol. Phys.* **2003**, *101*, 3477−3492.
(40) Keutsch, F. N.; Braly, L. B.; Brown, M. G.; Harker, H. A.; Petersen, P. B.; Leforestier, C.; Saykally, R. J. *J. Chem. Phys.* **2003**, *119*, 8927−8937.
(41) Zwart, E.; ter Meulen, J.; Meerts, W. L.; Coudert, L. *J. Mol. Spectrosc.* **1991**, *147*, 27−39.
(42) Fraser, G. T. *Int. Rev. Phys. Chem.* **1991**, *10*, 189−206.
(43) Paul, J. B.; Provencal, R. A.; Chapo, C.; Roth, K.; Casaes, R.; Saykally, R. J. *J. Phys. Chem. A* **1999**, *103*, 2972−2974.
(44) Huisken, F.; Kaloudis, M.; Kulcke, A. *J. Chem. Phys.* **1996**, *104*, 17−25.
(45) Buck, U.; Huisken, F. *Chem. Rev.* **2000**, *100*, 3863−3890.
(46) Kuyanov-Prozument, K.; Choi, M. Y.; Vilesov, A. F. *J. Chem. Phys.* **2010**, *132*, 014304.
(47) Nelander, B. *J. Chem. Phys.* **1988**, *88*, 5254−5256.
(48) Ceponkus, J.; Uvdal, P.; Nelander, B. *J. Phys. Chem. A* **2008**, *112*, 3921−3926.
(49) Huang, Z. S.; Miller, R. E. *J. Chem. Phys.* **1989**, *91*, 6613−6631.
(50) Harvey, A. H.; Lemmon, E. W. *J. Phys. Chem. Ref. Data* **2004**, *33*, 369−376.
(51) Duska, M.; Hrubý, J. *EPJ Web Conf.* **2013**, *45*, 01024.
(52) Applequist, J.; Carl, J. R.; Fung, K.-K. *J. Am. Chem. Soc.* **1972**, *94*, 2952−2960.
(53) Thole, B. *Chem. Phys.* **1981**, *59*, 341−350.
(54) Avila, G. *J. Chem. Phys.* **2005**, *122*, 144310.
(55) Ren, P.; Ponder, J. W. *J. Phys. Chem. B* **2003**, *107*, 5933−5947.
(56) Bartók, A. P.; Gillan, M. J.; Manby, F. R.; Csányi, G. *Phys. Rev. B* **2013**, *88*, 054104.